



Iron is Responsible for Production of Reactive Oxygen Species Regulating Vasopressin Expression in the Mouse Paraventricular Nucleus

Jong-A Hyeun^{1,4} · Ji Young Kim¹ · Chan Hyung Kim² · Jin-Hee Kim³ · Eun Young Lee¹ · Je Hoon Seo¹

Received: 14 August 2018 / Revised: 12 February 2019 / Accepted: 25 February 2019 / Published online: 4 March 2019
© Springer Science+Business Media, LLC, part of Springer Nature 2019

Abstract

Reactive oxygen species (ROS) act as signaling molecules for maintaining homeostasis, particularly in the regulation of body-fluid balance in the paraventricular nucleus (PVN) of the hypothalamus. However, there has been little discussion regarding the source of ROS generation in this hypothalamic region. Because iron is the most abundant metal in the brain, we hypothesized that iron may act as a source of ROS, which regulate vasopressin (VP) expression. In the present study, we compared the amount of iron in the PVN to that in other forebrain regions of normal ICR mice, and examined the relationship among iron, ROS, and VP in the PVN of the iron-overloaded with iron dextran and iron-chelated mice with deferoxamine. The amount of iron in the PVN was significantly higher than in any of the forebrain regions we examined. The amount of iron in the PVN was significantly increased in iron-overloaded mice, although not in iron-chelated mice. These results suggest that the PVN exhibits high iron affinity. Both ROS production and VP expression in the PVN of iron-overloaded mice were significantly increased relative to levels observed in control mice. VP concentration in blood of iron-overloaded mice was also significantly higher than that of control mice. Interestingly, iron overload did not alter the expression of nitric oxide synthase, another modulator of VP expression. Taken together, our results suggest that high levels of iron in the PVN induce the production of ROS, which regulate VP expression, independent of nitric oxide signaling.

Keywords Hypothalamus · Vasopressin · Magnocellular neuron · Iron dextran · Deferoxamine · Free radical

Electronic supplementary material The online version of this article (<https://doi.org/10.1007/s11064-019-02764-x>) contains supplementary material, which is available to authorized users.

✉ Je Hoon Seo
seojh@cbnu.ac.kr

¹ Department of Anatomy, Chungbuk National University College of Medicine, Chungdae-ro 1, Seowon-gu, Cheongju, Chungbuk 28644, Republic of Korea

² Department of Pharmacology, Chungbuk National University College of Medicine, Cheongju, Chungbuk 28644, Republic of Korea

³ Department of Biomedical Laboratory Science, College of Health Science, Cheongju University, Cheongju, Chungbuk 28503, Republic of Korea

⁴ Present Address: Department of Biochemistry, Chungbuk National University College of Medicine, Cheongju, Chungbuk 28644, Republic of Korea

Introduction

Reactive oxygen species (ROS) are hyperactive molecules formed via the mitochondrial electron transport chain of respiratory metabolism. Excess ROS can cause cellular damage that leads to lipid peroxidation, protein oxidation, and DNA/RNA modification [1]. Given their role in various pathological processes, ROS have been implicated in the onset and progression of neurodegenerative diseases [2], cancer [3], aging [4], myocardial infarction, and stroke [5]. However, ROS are essential for normal cellular function, playing key roles in the control of food intake [6, 7], the regulation of blood pressure and hypertension [8–10], synaptic plasticity and memory [11, 12], cell development [13], differentiation [14], and the early-induced innate and adaptive immune responses [15].

Iron is the most abundant metal in the brain, and brain iron can act as a source of ROS generation via iron-catalyzed reactions or enzyme activation. Several previous studies have demonstrated that high iron accumulation can generate

large amounts of ROS in the substantia nigra, cerebral cortex, hippocampus, and hypothalamus [16–20]. Hydroxyl radicals ($\cdot\text{OH}$), oxygen (O_2), and hydroxide ions (OH^-) can be formed from hydrogen peroxide (H_2O_2) and superoxide ($\cdot\text{O}_2^-$) via the Haber–Weiss reaction and Fenton reaction.

The paraventricular nucleus (PVN) of the hypothalamus is composed of magnocellular and parvocellular neurons. Magnocellular neurons in the PVN synthesize and liberate vasopressin (VP) into the neurohypophysis via the hypothalamohypophyseal tract [21]. Released VP is responsible for blood pressure control by vasoconstriction of smooth muscle cells and antidiuretic control by absorbing water from the renal tubules. In addition, VP has a multitude of functions involved in glycogenolysis in the liver, platelet aggregation, release of adrenocorticotrophic hormone in the adrenal gland [22]. Recent studies have suggested that ROS production is necessary for stimulating the VP response to osmoregulatory activity in the supraoptic nucleus (SON)—the connectivity, functions, and composition of which are similar to those of the PVN [21, 23]. Interestingly, previous investigators have reported that the SON and PVN are comparative iron-rich regions in the brain [24, 25]. Although there have not been reports about a direct association between iron levels and VP expression, high iron content in the PVN might be closely related to regulation of VP expression in this nucleus, considering that iron can act as a source of ROS generation. Therefore, we hypothesized that iron is responsible for the generation of ROS that regulate VP expression in the SON and PVN. To verify our hypothesis, we measured iron richness in the PVN and examined whether changes in iron levels can affect ROS generation and VP expression in iron-overloaded and iron-chelated mice.

Materials and Methods

Experimental Animals

Six week-old male ICR mice (30–32 g, $n = 100$) were obtained from a commercial source (DBL, Korea). Mice were housed under standard laboratory conditions under a 12 h light/dark cycle and were provided *ad libitum* access to a commercial diet and water. Mice were divided into three experimental groups: normal ($n = 10$), iron-overloaded ($n = 50$), and iron-chelated groups ($n = 40$). Iron-overloaded mice received an intraperitoneal injection of iron dextran (500 mg/kg, Sigma, USA), as previously described [18], and were sacrificed at 6 ($n = 10$), 12 ($n = 15$), and 48 h ($n = 10$) after injection. As a sham control, 15 mice were intraperitoneally injected with saline and sacrificed at 12 h. Iron-chelated mice were deeply anesthetized with a mixture of ketamine hydrochloride (100 mg/kg, Yuhan Co., Korea) and

xylazine hydrochloride (10 mg/kg, Bayer Korea, Korea). Each iron-chelated mouse was stereotaxically microinjected with deferoxamine (deferoxamine mesylate: 50 ng/ μl , Sigma, USA) into the lateral ventricle at a point 0.46 mm posterior and 1.0 mm lateral to the bregma (2.5 mm deep) in accordance with the mouse stereotaxic map, as previously described [18, 26]. Iron-chelated mice were sacrificed at 6, 12, and 48 h after injection ($n = 10$ each). As a sham control, 10 mice were stereotaxically microinjected with saline at the same point and sacrificed at 12 h. The present study was approved by the Institutional Animal Care and Use Committee at Chungbuk National University (Approval NO. CBNUA-092-0906-01). All procedures involving animals and animal care were conducted in accordance with the guidelines issued by the same committee.

Blood Sample Collection

Whole blood samples (50 μl) for enzyme-linked immunosorbent assay (ELISA) were drawn from the orbital plexuses of sham control ($n = 5$) and iron-overloaded mice (at 12 h after deferoxamine injection, $n = 5$) using heparinized capillary tubes (Kimble Chase, USA). We centrifuged whole blood samples at 1500 rpm for 10 min to obtain sera. All sera were stored at -80°C until used.

Tissue Preparation

Mice were deeply anesthetized with a mixture of ketamine hydrochloride and xylazine hydrochloride, following which they were transcardially perfused with precooled saline and 4% paraformaldehyde (PFA) in 0.1 M phosphate-buffered saline (PBS, pH 7.4). The brains were removed from the heads and postfixed in 4% PFA in cold room air (4°C) for 8 h. The brains were dehydrated in 30% sucrose in PBS overnight for cryoprotection. Brain tissues embedded in OCT compound (Leica, Germany) were rapidly frozen in 2-methyl butane (Junsei, Japan) adjusted to its freezing point with liquid nitrogen. Tissues were sectioned to a thickness of 50 μm using a cryostat (CM3050S, Leica, Germany). Consecutive coronal slices were collected in PBS and transferred to six-well plates. A series of coronal sections was placed in each well at intervals of 300 μm .

Detection of ROS

In situ detection of ROS was performed in accordance with protocols previously described [23]. Briefly, dihydroethidine (DHE, Invitrogen, USA) was diluted to 1 mg/ml in PBS and maintained at room temperature (RT, $22\text{--}25^\circ\text{C}$). Mice were sacrificed 12 h after intraperitoneal injection of 300 μl DHE. Mouse brains were sectioned to a thickness of 40 μm using a cryostat. The sections were washed in PBS, following which

they were incubated with DHE (1 μ M in PBS) for 5 min at RT in total darkness. Following incubation, the sections were washed three times (5 min each) in PBS. The sections were coverslipped with aqueous mounting medium (Biomeda, USA), and the fluorescence intensities of ROS were analyzed using a multipurpose microscope with an epifluorescence attachment (DMLB, Leica, Germany).

Iron Histochemistry and Nissl Staining

Iron histochemistry, known as Pearl's histochemistry is a well-established staining method to visualize localization of iron in the tissue [27]. We performed iron histochemistry to identify the regional distribution of iron in the forebrain, in accordance with protocols previously described [17]. Briefly, the sectioned tissues were washed in Milli-Q ultrapure water and incubated in iron staining solution (4% potassium ferrocyanide: 2% Triton X-100: 5N HCl = 1:2:1) for 2 h. The sections were then rinsed in PBS and reacted with 0.2% 3,3'-diaminobenzidine (DAB) in PBS containing 0.1% hydrogen peroxide. Iron-stained sections were mounted on gelatin-coated slides and air-dried. The stained sections were dehydrated, cleared, and coverslipped with mounting medium (Permount, Fisher Scientific, USA). To confirm the localization and subdivision of the PVN, Nissl staining was performed using 1% cresyl violet solution (Sigma, USA). Stained sections were dehydrated, cleared, coverslipped, and examined using a multipurpose microscope (DMLB, Leica, Germany) equipped with a digital camera system (Macrofire, Optronics, USA).

Immunohistochemistry

The sections were incubated with 0.3% hydrogen peroxide in methanol for 20 min to quench endogenous peroxidase activity. Then, the sections were pre-blocked in 10% normal goat serum for 30 min and incubated with rabbit anti-VP antibody (1:5000; Chemicon International, USA), rabbit anti-gamma-aminobutyric acid (GABA) transaminase antibody (1:50; Abcam, USA), and mouse anti- α B-crystalline (aBC, 1:200; Stressgene, USA) for an oligodendrocyte marker diluted in PBS in 4 °C cold room air. Subsequently, we performed the avidin–biotin peroxidase complex method, as previously described [28]. Briefly, the sections were incubated in biotinylated goat anti-rabbit immunoglobulin G (IgG) (Vector Laboratories, USA) or goat anti-mouse IgG (Vector Laboratories, USA) diluted at 1:400 in PBS for 2 h at RT. The sections were washed three times for 10 min each in PBS and incubated in the avidin–biotin peroxidase complex (ABC Elite kit, Vector Laboratories). The peroxidase reaction was visualized using 0.2% DAB in PBS containing 0.1% hydrogen peroxide, following which the sections were dehydrated and coverslipped with mounting medium.

For negative controls, either primary or secondary antisera were omitted during immunohistochemical staining. Following iron histochemical staining, we performed immunohistochemistry to identify specific types of iron-positive cells. We used anti-VP and anti-aBC antibodies to detect magnocellular neurons and oligodendrocytes, respectively. Immunoreactivity was visualized using an SG peroxidase substrate kit (Vector Laboratories, USA).

Sandwich ELISA

VP concentration in sera was determined by the sandwich ELISA method as previously described [29]. Briefly, 96-well ELISA plates (Nunc, USA) were coated with mouse anti-VP antibody (1:1000; EMD Millipore, USA) and blocked with 1% skim milk in PBS. Sera (1:100 dilution) were added to each well and incubated for 2 h at RT. To each well, 3 μ g/100 μ l of horseradish peroxidase (HRP)-conjugated secondary antibody was added for 1 h at RT. A color reaction and interruption of reaction were performed by adding 50 μ l of substrate solution (2 μ g/100 μ l of 3,3',5,5'-tetramethylbenzidine, Sigma, USA) and 50 μ l of stop solution (Southern Biotech, USA), respectively. The absorbance was measured at 450 nm using a microplate spectrophotometer (SpectraMax M5e, Molecular Devices, USA). We used SoftMax Pro 5.4.1 (Molecular Devices, USA) for the analysis.

NADPH-Diaphorase Staining

NADPH-diaphorase positive neurons were detected as previously described [30]. The sections were washed in PBS and incubated in NADPH-diaphorase staining mixture for 1 h at 37 °C (1 mg/ml β -NADPH, 0.3 mg/ml nitroblue tetrazolium, 0.3% Triton X-100 in PBS). Following incubation, stained sections were rinsed three times for 10 min each in PBS and mounted on gelatin-coated slides, dehydrated, cleared, coverslipped, and examined using a multipurpose microscope (DMLB, Leica, Germany).

TUNEL and Hematoxylin Staining

To examine whether iron-overloaded mice exhibited increased neuronal damage in the PVN, we performed terminal deoxynucleotidyl transferase dUTP nick end labeling (TUNEL) in accordance with previously described methods [31]. Briefly, the sections were incubated with TUNEL labeling mix (Roche, Germany) containing 0.135 U/ μ l calf thymus terminal deoxynucleotidyl transferase (TdT), 0.0044 nmol/ μ l digoxigenin-11-2'-deoxy-uridine-5'-triphosphate (DIG-dUTP), and 1 mM cobalt chloride for 1 h at 37 °C in a moist chamber. Following incubation, the sections were washed in Tris-buffered saline (TBS, pH 7.4) for 10 min and then blocked with 1% blocking buffer for

30 min. They were then incubated with mouse anti-DIG antibody (1:500, Roche, Germany) in 1% blocking buffer for 1 h at 37 °C. The sections were washed in PBS for 10 min and incubated with peroxidase-labelled mouse IgG for 1 h at RT. The tissues were then rinsed in PBS and reacted with 0.2% DAB in PBS containing 0.1% hydrogen peroxide. The other sections for histologic examination were stained with hematoxylin. Hematoxylin staining was used to detect pyknotic nuclei. The stained sections were coverslipped with mounting medium, dehydrated, and analyzed using a multipurpose microscope (DMLB, Leica, Germany) equipped with a digital camera system (Macrofire, Optronics, USA).

Cell Size Analysis

To determine whether iron-stained cells in the PVN were magnocellular or parvocellular neurons, we examined the distribution of cell diameter (%) in cresyl violet-stained and iron-stained neurons. Microphotographs for cell size analysis were taken at the same magnification using a multipurpose microscope (DMLB, Leica, Germany). The diameters of the cresyl violet-stained and iron-stained neurons in the PVN were analyzed using i-Solution DT (IMT, Korea). We calculated the percentage of cells with the same diameter between 5 and 20 μm , using intervals of 1 μm . Cell size data were obtained from 14 sections acquired from 10 brains of normal mice.

Optical Density and Cell Count

The optical densities (ODs) of iron-stained sections were measured to determine iron reactivity in several forebrain regions, including the PVN. We standardized and analyzed the images captured from iron-stained sections. We first converted the captured RGB color images to grayscale, following which the grayscale images were inverted using Photoshop CS5 (Adobe, USA). Then, the gray values (0–255) of the inverted grayscale images were standardized by subtracting the background gray values. We outlined the specific regions in the standardized gray images as outlined in Fig. 3a and obtained the gray values in the outlined regions using i-Solution. The relative gray values were regarded as the ODs. Increases and decreases in OD were calculated as follows: $((\text{OD}_{\text{overload}} - \text{OD}_{\text{control}}) / \text{OD}_{\text{control}}) \times 100$ and $((\text{OD}_{\text{control}} - \text{OD}_{\text{chelation}}) / \text{OD}_{\text{control}}) \times 100$, respectively.

We counted the numbers of VP positive, NADPH-d positive, TUNEL positive and pyknotic cells to determine change in number of these cells in iron-overloaded mice. We first outlined the PVN and measured its size. Then, we counted the numbers of these cells in the outlined PVN. Finally, we calculated the number of cells per mm^2 to standardize the counts.

Statistical Analysis

Results were expressed as the mean \pm standard error of the mean (SEM). The significances of differences were determined using Student's t-tests or analyses of variance (ANOVA), followed by Bonferroni post hoc tests. All analyses were performed using Prism 4 (GraphPad, USA). P-values less than 0.01 were deemed statistically significant.

Results

Iron Histochemistry

The location and subdivisions of the PVN were identified via cresyl violet staining. The neurons in the PVN were densely gathered adjacent to the third ventricle (Fig. 1a). The PVN exhibited strong iron reactivity (Fig. 1b). Iron reactivity was detected in almost all neurons in the compact (Fig. 1c) and medial parts (Fig. 1d) of the PVN. With the exception of scattered iron-reactive cells with small, round cell bodies, iron reactivity was not observed outside the PVN (Fig. 1e). Iron histochemical staining patterns remained unchanged and were very similar in repeated experiments, indicating that the iron staining method we performed was reproducible.

Double staining using iron histochemistry and immunohistochemistry showed that most iron-reactive cells in the PVN exhibited VP immunoreactivity, suggesting that these cells were magnocellular neurons (Fig. 2a). In contrast, iron-reactive round cells outside the PVN exhibited aBC immunoreactivity, suggesting that these cells were oligodendrocytes (Fig. 2b).

Comparison of Iron Reactivity in Forebrain Regions

Strong iron reactivity was observed in several regions throughout the forebrain (Fig. 3a), including the PVN, anteroventral nucleus (AV), lateral hypothalamic area (LH), globus pallidus (GP), and thalamic nucleus reuniens (Re). Under high magnification, we examined the cell shapes of iron-reactive cells in these iron-rich regions. Except for the PVN, iron-reactive cells in all regions had small, round cell bodies (Fig. 3b–e). The shape of these small, iron-reactive cells was very similar to that of iron-reactive oligodendrocytes in the corpus callosum and internal capsule, which are the main white matter regions of the brain (Fig. 3f, g). These findings suggest that the iron-reactive cells in the AV, LH, GP, and Re with small, round cell bodies were oligodendrocytes rather than neurons. In addition, our results indicated

Fig. 1 Iron histochemistry and cresyl violet staining. **a** Cresyl violet staining. Neurons of the PVN (in dotted line) are located adjacent to the third ventricle. **b** Iron histochemical staining. Almost all cells of the PVN are strongly iron-stained. **c-e**: High-magnification images of boxed areas in **b**. All neurons in the compact (**c**) and medial parts (**d**) of the PVN exhibited strong iron reactivity. Small, round iron-reactive cells are scattered outside the PVN (**e**). 3V, third ventricle; cp, compact part; mp, medial part. Scale bar in **e** for **a**, **b** = 200 μm , for **c-e** = 40 μm

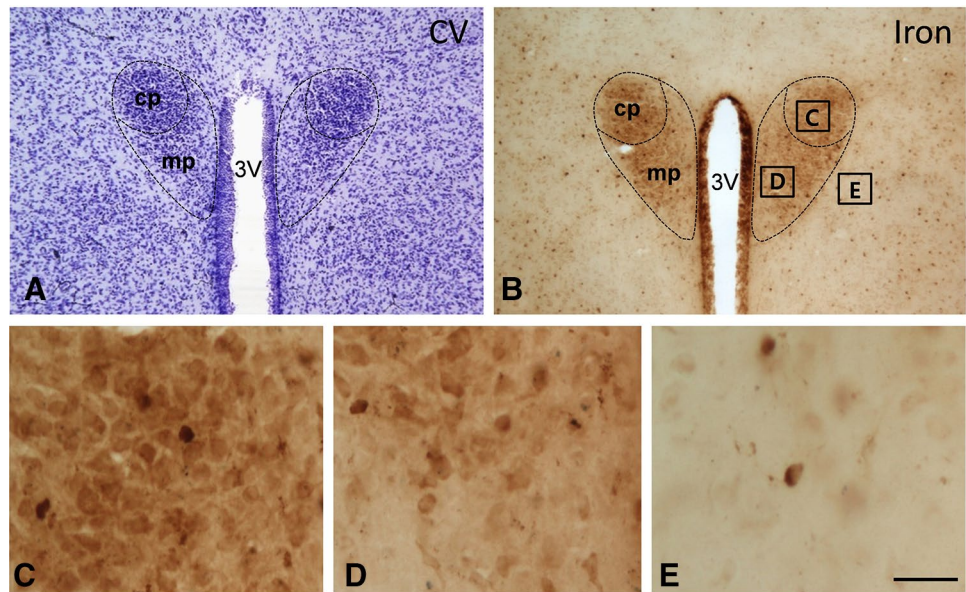
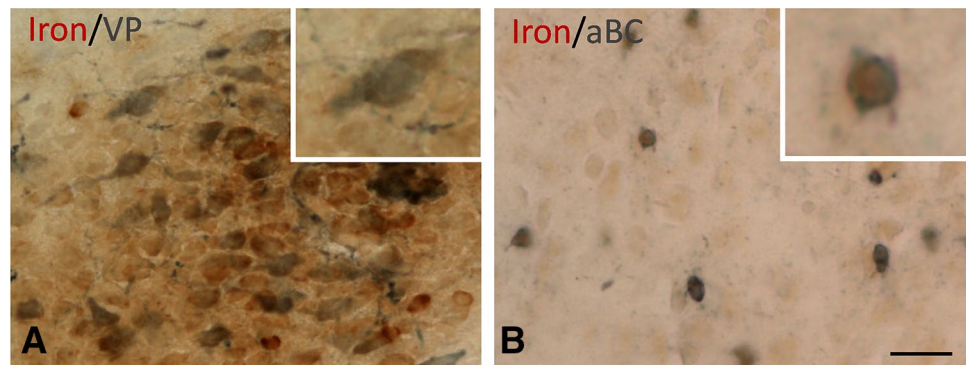


Fig. 2 Double-staining using iron histochemistry and immunohistochemistry. **a** Iron and VP in the PVN. Most VP-positive neurons (dark gray) exhibited iron reactivity (brown). **b**: Iron and aBC outside the PVN. All aBC-positive oligodendrocytes (dark gray) also exhibited strong iron reactivity (brown). Inserts show the magnifications of **a** and **b**. Scale bar for **a**, **b** = 50 μm . (Color figure online)



that ODs in the PVN were significantly higher than those in other forebrain regions (Fig. 3h).

Iron Reactivity in Iron-Overloaded and Iron-Chelated Mice

We examined iron reactivity in iron-overloaded mice. The OD of the PVN was significantly at 6 and 12 h after iron dextran injection, although it recovered to normal levels at 48 h after injection (Fig. 4a). The ODs of the other brain regions except the PVN did not reach to significant increases (Fig. 4a). We then compared rates of OD increase among regions at 12 h after injection. The rate of OD increase in the PVN was approximately 28% at 12 h after injection. However, rates of increase were less than 20% in other regions (Fig. 4b).

We also examined iron reactivity in iron-chelated mice. Although the OD of the PVN tended to be decreased for up to 6 h and recover by 48 h after deferoxamine injection, these

differences were not significant (Fig. 5a). We then compared rates of OD decrease among regions at 12 h after injection. The OD of the PVN was decreased to approximately 10% at 12 h after injection. However, the ODs in other regions were significantly decreased to approximately 20% at 12 h after injection (Fig. 5b). Taken together, these results indicate that the PVN has a higher affinity for iron than any other forebrain region.

Cell Size Analysis

We determined whether most iron-stained neurons were magnocellular or parvocellular neurons by comparing cell size distribution between cresyl violet-stained and iron-stained neurons. The diameters of cresyl violet-stained neurons, which consist of both magnocellular and parvocellular neurons, ranged from 5 μm to 20 μm . The distribution of cell diameters was very similar between iron-stained and

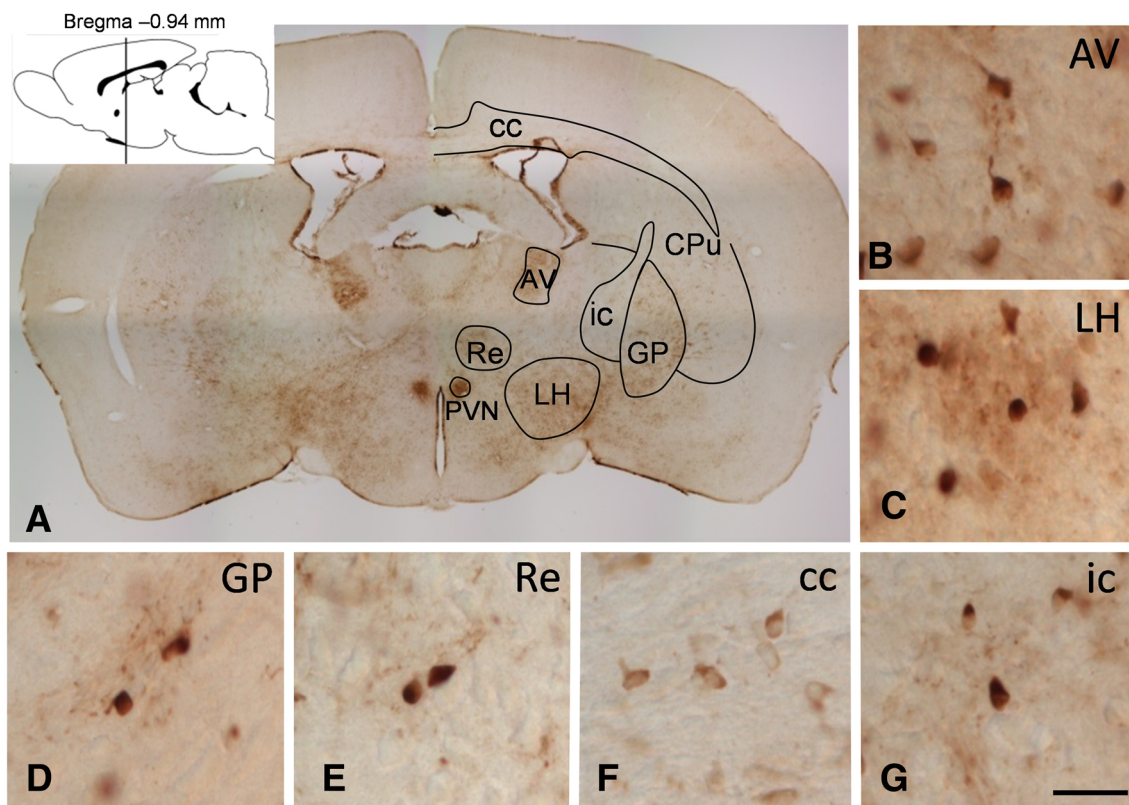


Fig. 3 Iron reactivity and ODs. **a** Coronal forebrain sections stained for iron at -0.94 mm to bregma. **b–g** High magnification images of several regions in **a**. Scattered iron-reactive cells have small, round cell bodies in the anteroventral nucleus (**b**), lateral hypothalamic area (**c**), globus pallidus (**d**), thalamic nucleus reuniens (**e**), corpus callosum (**f**), and internal capsule (**g**). **h** Comparison of ODs among fore-

brain regions. The OD of the PVN is much higher than those of other regions. AV, anteroventral nucleus; cc, corpus callosum; CPu, caudate putamen; GP, globus pallidus; ic, internal capsule; LH, lateral hypothalamic area; Re, thalamic nucleus reuniens; PVN, paraventricular nucleus. Scale bar in **g** for **a** = 400 μ m, for **b–g** = 25 μ m

resyl violet-stained neurons (Fig. 6), and there was no significant difference between the two. This result means that iron-stained cells in the PVN include both magnocellular and parvocellular neurons.

ROS Production and VP Expression in Magnocellular Neurons

We evaluated the relationships between ROS production and VP expression in iron-overloaded and iron-chelated

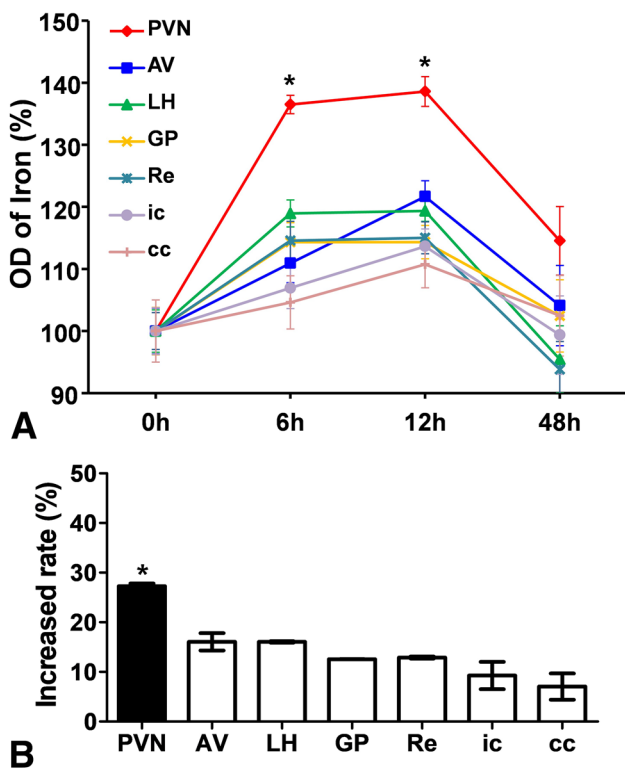


Fig. 4 Iron-overloaded mice. **a** Time-dependent changes. The OD of iron in the PVN was significantly increased at 6 h and 12 h after iron dextran injection. **b** Rates of OD increase at 12 h after iron dextran injection. Rates of OD increase were significantly higher in the PVN than in other forebrain regions. Asterisks in **a** indicate significant differences versus 0 h. Asterisk in **b** indicates significant differences versus the rate observed in the PVN (**p* < 0.01)

mice. Iron reactivity was significantly increased in the PVN of iron-overloaded mice (Fig. 7a, b, d), along with ROS production (Fig. 7e, f, h) and VP expression (Fig. 7i, j, l). Relative to controls, iron-overloaded mice exhibited an approximately 30% increase in OD in the PVN (Fig. 7d). Similarly, ROS production and VP expression were increased by approximately 30% in iron-overloaded mice (Fig. 7h, l). However, iron reactivity remained unchanged in the PVN of iron-chelated mice (Fig. 7a, c, d). Furthermore, iron-chelated mice exhibited no changes in ROS production (Fig. 7e, g, h) or VP expression (Fig. 7i, k, l). These data suggest that the production of ROS that regulate VP expression results from iron accumulation in the PVN.

VP Concentration in Blood

To investigate the VP concentration in sera, relative sandwich ELISA was conducted in control and iron-overloaded groups. The results showed that the VP concentration in the sera from the iron-overloaded mice was significantly

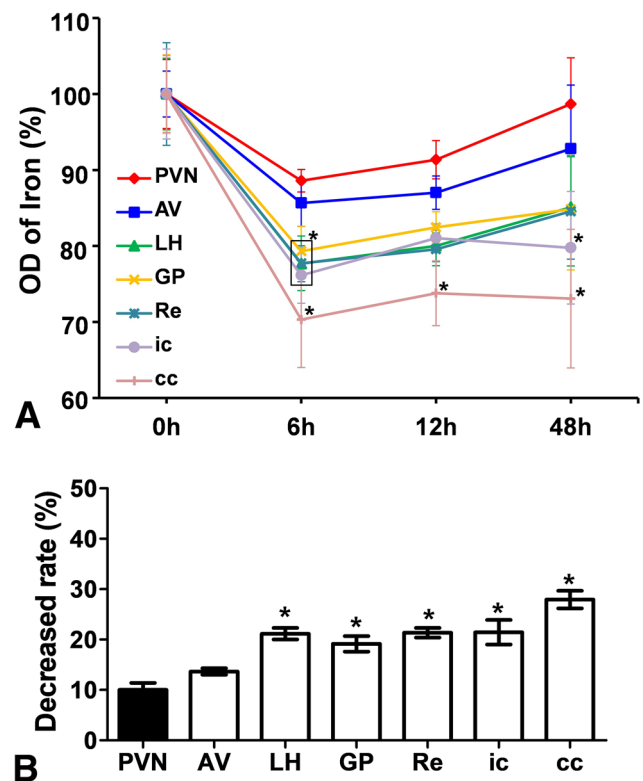


Fig. 5 Iron-chelated mice. **a** Time-dependent changes. The OD of iron in the PVN remained unchanged after deferoxamine injection. **b** Rates of OD decrease at 12 h after deferoxamine injection. Rates of OD decrease were significantly lower in the PVN than in other forebrain regions. Asterisks in **a** indicate significant differences versus 0 h. Asterisks in **b** indicate significant differences versus the rate observed in the PVN (**p* < 0.01)

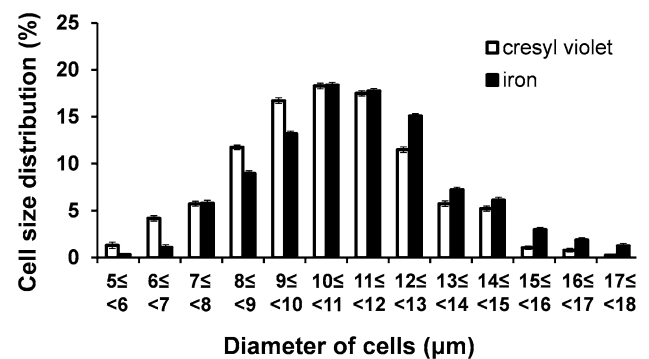


Fig. 6 Cell size distribution. There were no significant differences in cell size distribution between iron-stained cells and cresyl violet-stained neurons (two-way ANOVA), indicating that iron-stained cells in the PVN included both magnocellular and parvocellular neurons

increased, compared with that from the controls (Fig. 8). This result means that iron overload increases not only VP expression the magnocellular neurons, but also VP release into blood.

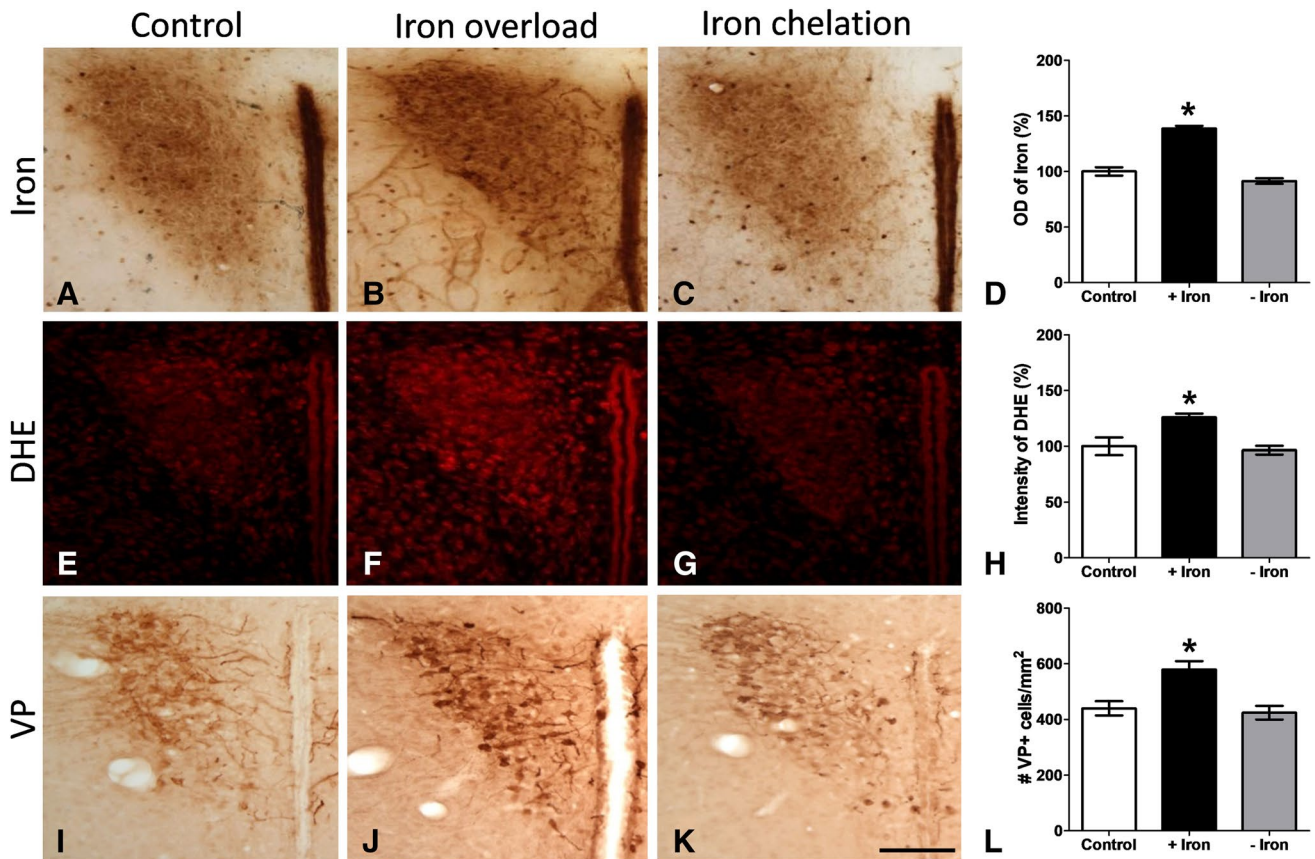


Fig. 7 Iron, ROS, and VP expression in iron-overloaded and iron-chelated mice. The amount of iron was significantly increased in the PVN of iron-overloaded mice (**a, b, d**). ROS production (**e, f, h**) and VP expression (**i, j, l**) were also increased in iron-overloaded mice. However, the amount of iron remained unchanged in the PVN of

iron-chelated mice (**a, c, d**), along with ROS (**e, g, h**) and VP expression (**i, k, l**). Scale bar = 100 μ m. + Iron and - Iron mean iron overload and iron chelation, respectively. Asterisks indicate significant differences among the three groups (* $p < 0.01$)

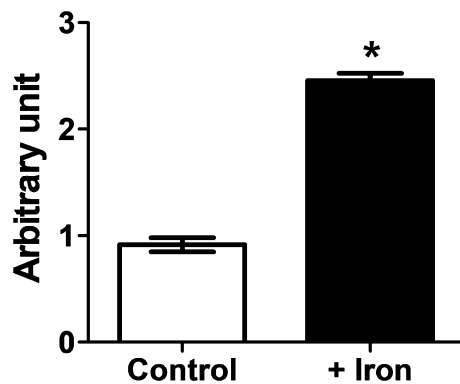


Fig. 8 VP concentration in blood of iron-overloaded mice. Relative VP concentration in the blood of iron-overloaded mice was significantly increased compared with that of the controls (* $p < 0.01$). + Iron means iron overload

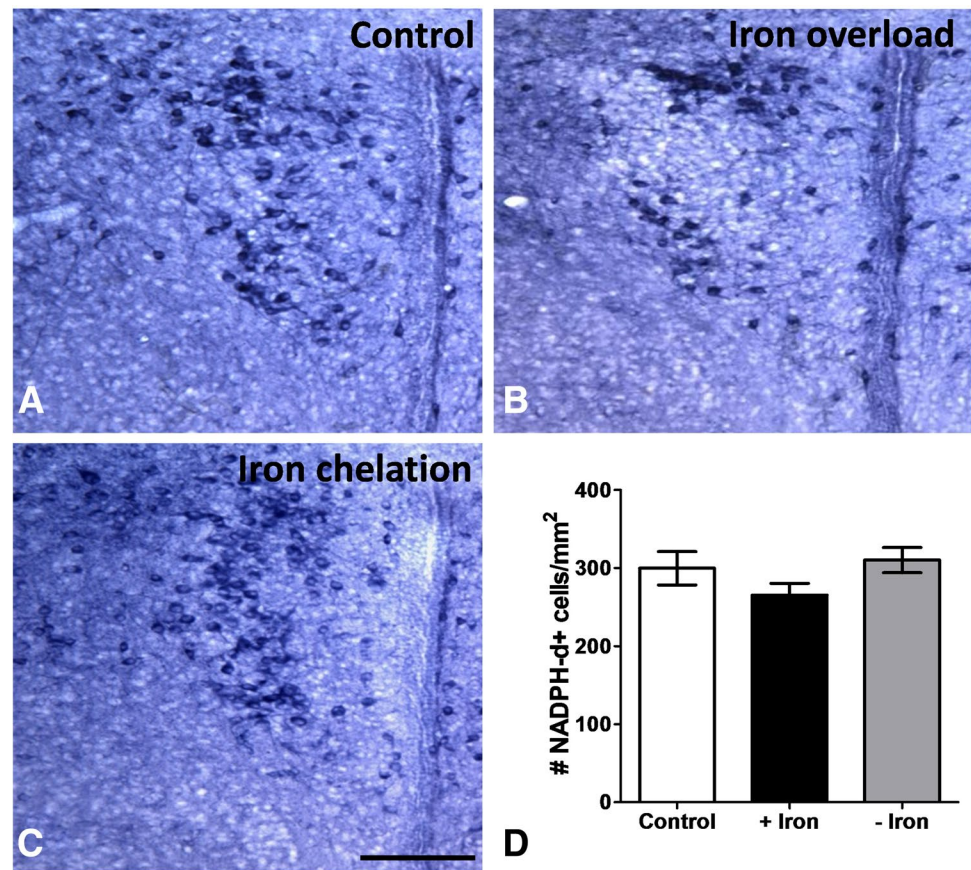
NADPH-Diaphorase Expression in Magnocellular Neurons

To determine whether changes in iron accumulation in the PVN can affect the production of nitric oxide (NO), another regulator of VP expression, we examined the expression of nitric oxide synthase (NOS) via NADPH-diaphorase histochemistry. There were no significant differences in NOS expression among the control, iron-overloaded, and iron-chelated mice (Fig. 9a–d). This result suggests that iron is not involved in osmoregulation via the NO signaling pathway.

GABA Transaminase Expression in Parvocellular Neurons

We examined whether GABA transaminase expression in parvocellular neurons was altered in iron-overloaded and iron-chelated mice. There were no significant differences in GABA transaminase expression among the control,

Fig. 9 NADPH-diaphorase expression in iron-overloaded and iron-chelated mice. No significant differences in NOS expression were observed among the three groups (a–d). Scale bar for a–c = 100 μ m. +Iron and -Iron mean iron overload and iron chelation, respectively



iron-overloaded, and iron-chelated mice (Fig. 10a–d). This result suggests that changes in iron accumulation do not affect GABA transaminase expression in parvocellular neurons of the PVN.

Detection of Cell Death in the PVN

We examined whether changes in the amount of ROS in the PVN were associated with changes in levels of cell death via TUNEL and hematoxylin staining. No TUNEL-positive cells were detected in either control or iron-overloaded mice (Fig. 11a–c). Upon histologic examination, a few cells in the PVN exhibited condensed nuclei, a sign of cell death, in both control and iron-overloaded mice (Fig. 11d, e). However, no significant differences were observed between the two groups (Fig. 11f). These data suggest that iron-induced increases in ROS do not induce cell death in the PVN.

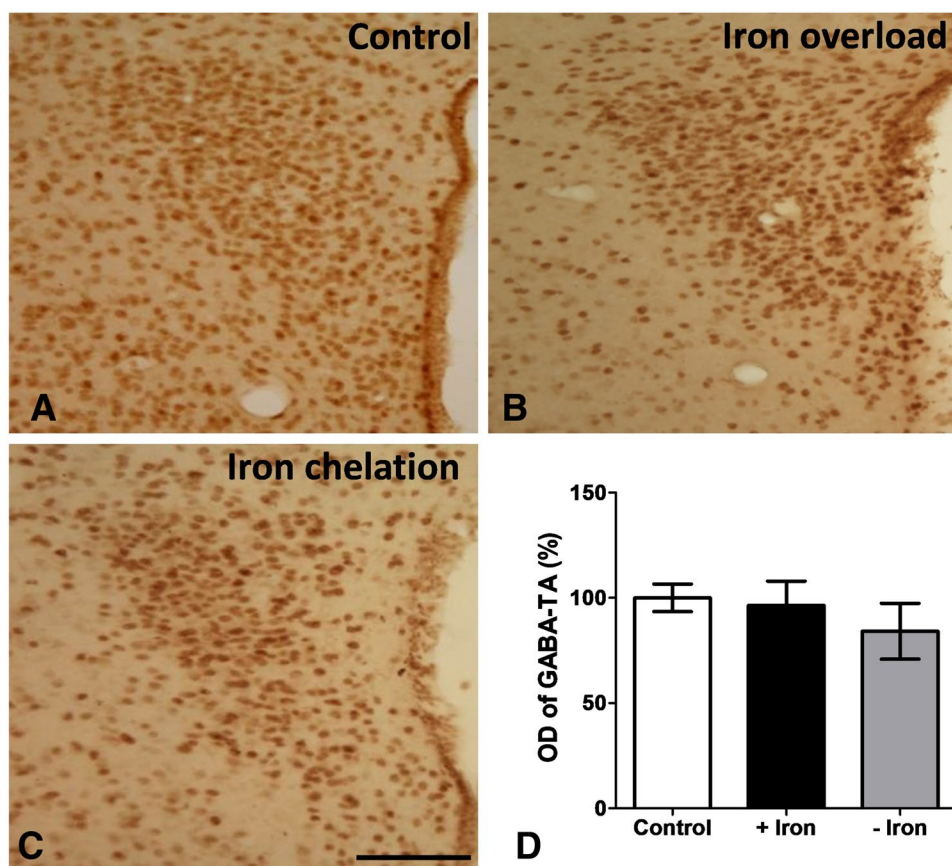
Discussion

In the present study, we examined whether changes in iron levels can affect ROS generation and VP expression in iron-overloaded and iron-chelated mice. Our results demonstrated that iron accumulation was greater in the PVN than in any

other forebrain region. Furthermore, we observed that the PVN tended to maintain high iron affinity in iron-overloaded and iron-chelated mice. High iron affinity of the PVN led to significant increase of iron levels in iron-overloaded mice. However, in the iron-chelated mice, high iron affinity of the PVN did not cause a change in iron levels. As a result, excessive ROS were generated by increased iron in the PVN of iron-overloaded mice. These results suggest that iron levels are directly correlated with ROS generation. We speculate that abundant iron in the PVN generates ROS via the Fenton reaction, which forms hydroxide (OH^-) and hydroxyl radicals ($\cdot\text{OH}$). The PVN has the underlying mechanism to regulate excessive ROS induced by abundant iron. The magnocellular neurons contain ferritin mRNA and protein [32, 33]. Ferritin binds toxic free iron and stores iron in a stable state. If necessary, iron can be easily released from ferritin. Release of iron from ferritin is mediated by intracellular glutathione, xanthine oxidase, reduced flavins, and superoxide [34]. Thus, ferritin can precisely regulate ROS formation by binding iron.

Previous studies demonstrated that ROS play crucial role in the control of physiological regulation of VP expression in magnocellular neurons of the hypothalamus [21, 23]. Although the signaling pathway through which ROS regulate VP expression is still unclear, it is well known that ROS

Fig. 10 GABA transaminase expression in iron-overloaded and iron-chelated mice. No significant differences in GABA transaminase expression were observed among the three groups. Scale bar for a-c = 100 μ m. + Iron and - Iron mean iron overload and iron chelation, respectively. GABA-TA, GABA transaminase



serve in signaling pathways of various cellular processes including cell proliferation, survival, and antioxidant regulation. ROS interact with crucial signaling molecules such as the mitogen-activated protein kinase (MAPK), phosphoinositide 3-kinase (PI3 kinase), protein kinase C (PKC), phosphatase and tensin homolog (PTEN), and nuclear factor erythroid 2-related factor 2 (Nrf2). The cGMP-dependent protein kinase (PKG) regulating MAPK activation is a redox sensor activated by ROS [35]. Through PTEN oxidized by ROS, the PI3K pathway is regulated [35]. Oxidation of cysteines in Kelch-like ECH-associated protein-1 (Keap1) by ROS causes Nrf2 release from the Keap1-Nrf2 complex. Subsequently, Nrf2 undergoes nuclear translocation and binds the antioxidant-responsive element [35]. The PKC is also regulated through redox mechanisms [36]. Emerging evidence indicates that the PKC activation increases the VP expression through the c-Fos-mediated pathway [37]. Therefore, it is conceivable that abundant ROS induced by iron accumulation in the PVN regulates the PKC pathway, which results in the VP gene activation.

Although there were no changes in iron, ROS, or VP expression in the PVN of iron-chelated mice in the present study, our findings demonstrated that iron overload produces excessive ROS, in turn leading to increases in VP expression

in magnocellular neurons. It is well known that magnocellular neurons in the SON and PVN are responsible for VP expression [21]. We also observed iron accumulation in the SON (Fig. S1). However, as we did not examine whether iron accumulation affects ROS production and VP expression in the SON, further studies are required. Future studies should also aim to examine the influence of iron-induced increases in ROS signaling on the production of oxytocin in magnocellular neurons.

Our cell size analysis indicated that both magnocellular and parvocellular neurons in the PVN contain large amounts of iron. These findings are in accordance with those of previous electron microscopic studies [25], which have suggested that the expression of GABA transaminase can be affected by iron accumulation in parvocellular neurons [25], since this enzyme contains iron-sulfur bonds at the center [38]. They also presumed that the postsynaptic parvocellular neurons have strong iron demand, because GABA transaminase plays a crucial role in the degradation of GABA in the PVN with strong GABAergic inhibitory inputs. Therefore, we anticipated that iron overload would increase GABA transaminase expression in the parvocellular neurons. However, we observed no significant differences in GABA transaminase expression between the control and iron-overloaded mice.

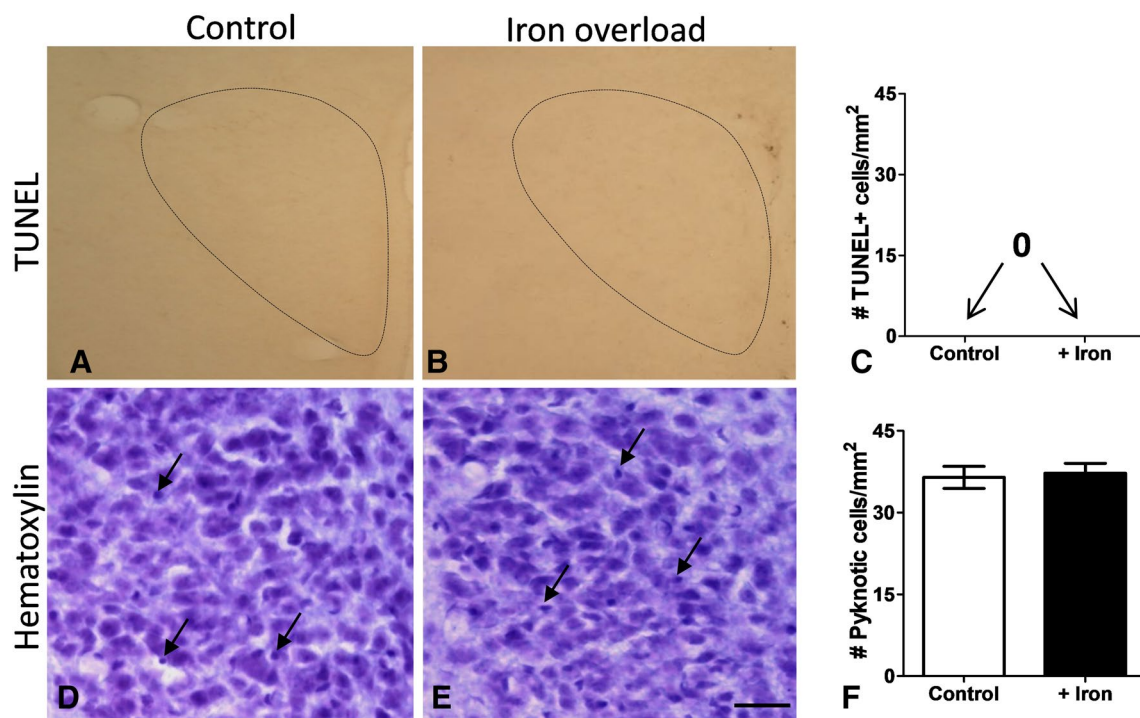


Fig. 11 Cell death in the PVN of iron-overloaded mice. No TUNEL-positive cells were detected in the PVN of control or iron-overloaded mice (a–c). A few cells with condensed nuclei were observed in the hematoxylin-stained PVN (arrows in d, e), although there were no

significant differences in cell death between the control and iron-overloaded groups (f). Scale bar in e for a and b = 100 μ m, d and e = 25 μ m. + Iron means iron overload

Our result reflects that the GABA transaminase expression is controlled differently than VP expression in terms of ROS that are induced by iron accumulation. Although parvocellular neurons contribute to homeostasis via the hypothalamo-hypophyseal portal system, few studies have examined the relationship between iron accumulation and parvocellular neurons. Therefore, future studies should investigate additional iron-related enzymes as well as the role of iron in parvocellular neurons.

Previous researchers have proposed that VP expression in the PVN is regulated by NO, which acts as a gaseous messenger molecule. Indeed, previous studies have reported that NOS expression is directly correlated with VP and oxytocin expression in the rat PVN and SON [39–41]. Thus, we examined changes in NOS expression in iron-overloaded mice. Despite increases in VP expression, iron overload did not increase NOS expression. Taken together, these findings strongly suggest that VP expression is regulated by at least two independent pathways (i.e., iron-related ROS and non-iron-related NO signaling).

Like a double-edged sword, abundant iron in the PVN may be responsible for susceptibility to harmful oxidative damage as well as the production of ROS to control osmoregulation in the body. Iron accumulation in neurons is an abnormal phenomenon, and is often observed in patients

with neurodegenerative conditions such as Parkinson's disease and Alzheimer's disease [42, 43]. Brain iron is commonly restricted within glial cells such as oligodendrocytes, microglia, and Bergmann glia [17, 44]. Interestingly, iron overload in PVN neurons did not result in increased cell death in the present study, in accordance with previous findings: High levels of antioxidants in the SON—which is identical to the PVN in terms of cell composition, connectivity, and hormone production—are known to prevent oxidative damage [23]. Another study demonstrated that the numbers of magnocellular neurons in the PVN do not decrease during aging in mice [45]. Taken together, these findings suggest that the PVN is highly stable and resistant to oxidative damage, promoting cell survival.

In summary, our results indicated that both magnocellular and parvocellular neurons in the PVN exhibited abundant iron accumulation, and that the PVN exhibits higher iron affinity than any other forebrain region. Iron overload in the PVN increased ROS production, in turn increasing VP expression in magnocellular neurons. However, iron overload did not alter GABA transaminase or NOS expression. Our results suggest that iron in the PVN is responsible for the production of ROS that regulate VP expression, and that this pathway is independent of NO signaling.

Acknowledgements This research was supported by the Basic Science Research Program through the National Research Foundation of Korea (NRF) funded by the Ministry of Education, Science and Technology (NRF-2013R1A1A2011095), and the intramural research grant of Chungbuk National University in 2015.

Compliance with Ethical Standards

Conflict of interest None of the authors have any conflicts of interest to declare.

References

- Pereira RD, De Long NE, Wang RC, Yazdi FT, Holloway AC, Raha S (2015) Angiogenesis in the placenta: the role of reactive oxygen species signaling. *BioMed Res Int* 2015:814543
- Barnham KJ, Masters CL, Bush AI (2004) Neurodegenerative diseases and oxidative stress. *Nat Rev Drug Discov* 3:205–214
- Waris G, Ahsan H (2006) Reactive oxygen species: role in the development of cancer and various chronic conditions. *J Carcinog* 5:14
- Poon HF, Calabrese V, Scapagnini G, Butterfield DA (2004) Free radicals: key to brain aging and heme oxygenase as a cellular response to oxidative stress. *J Gerontol Ser A* 59:478–493
- Kalogeris T, Bao Y, Korthuis RJ (2014) Mitochondrial reactive oxygen species: a double edged sword in ischemia/reperfusion vs preconditioning. *Redox Biol* 2:702–714
- Benani A, Troy S, Carmona MC, Fioramonti X, Lorsignol A, Leloup C, Casteilla L, Penicaud L (2007) Role for mitochondrial reactive oxygen species in brain lipid sensing: redox regulation of food intake. *Diabetes* 56:152–160
- Leloup C, Magnan C, Benani A, Bonnet E, Alquier T, Offer G, Carriere A, Periquet A, Fernandez Y, Ktorza A, Casteilla L, Penicaud L (2006) Mitochondrial reactive oxygen species are required for hypothalamic glucose sensing. *Diabetes* 55:2084–2090
- Abboud F, Floras J, Aylward P, Guo G, Gupta B, Schmid P (1990) Role of vasopressin in cardiovascular and blood pressure regulation. *J Vasc Res* 27:106–115
- Wang G, Coleman CG, Chan J, Faraco G, Marques-Lopes J, Milner TA, Guruju MR, Anrather J, Davissou RL, Iadecola C, Pickel VM (2013) Angiotensin II slow-pressor hypertension enhances NMDA currents and NOX2-dependent superoxide production in hypothalamic paraventricular neurons. *Am J Physiol Regul Integr Comp Physiol* 304:R1096–R1106
- Xia H, Suda S, Bindom S, Feng Y, Gurley SB, Seth D, Navar LG, Lazartigues E (2011) ACE2-mediated reduction of oxidative stress in the central nervous system is associated with improvement of autonomic function. *PLoS ONE* 6:e22682
- Hidalgo C, Carrasco MA, Munoz P, Nunez MT (2007) A role for reactive oxygen/nitrogen species and iron on neuronal synaptic plasticity. *Antioxid Redox Signal* 9:245–255
- Kishida KT, Klann E (2007) Sources and targets of reactive oxygen species in synaptic plasticity and memory. *Antioxid Redox Signal* 9:233–244
- Yang Y, Bazhin AV, Werner J, Karakhanova S (2013) Reactive oxygen species in the immune system. *Int Rev Immunol* 32:249–270
- Ji AR, Ku SY, Cho MS, Kim YY, Kim YJ, Oh SK, Kim SH, Moon SY, Choi YM (2010) Reactive oxygen species enhance differentiation of human embryonic stem cells into mesodermal lineage. *Exp Mol Med* 42:175–186
- Spooner R, Yilmaz O (2011) The role of reactive-oxygen-species in microbial persistence and inflammation. *Int J Mol Sci* 12:334–352
- Gerlach M, Ben-Shachar D, Riederer P, Youdim MB (1994) Altered brain metabolism of iron as a cause of neurodegenerative diseases. *J Neurochem* 63:793–807
- Kim JY, Lee EY, Sohn HJ, Kim DW, Cho SS, Seo JH (2014) Sequential accumulation of iron in glial cells during chicken cerebellar development. *Acta Histochem* 116:570–576
- Jiang H, Luan Z, Wang J, Xie J (2006) Neuroprotective effects of iron chelator desferal on dopaminergic neurons in the substantia nigra of rats with iron-overload. *Neurochem Int* 49:605–609
- Sofic E, Riederer P, Heinsen H, Beckmann H, Reynolds GP, Hebenstreit G, Youdim MB (1988) Increased iron (III) and total iron content in post mortem substantia nigra of parkinsonian brain. *J Neural Transm* 74:199–205
- Mesquita SD, Ferreira AC, Sousa JC, Santos NC, Correia-Neves M, Sousa N, Palha JA, Marques F (2012) Modulation of iron metabolism in aging and in alzheimer's disease: relevance of the choroid plexus. *Front Cell Neurosci* 6:25
- St-Louis R, Parmentier C, Grange-Messent V, Mhaouty-Kodja S, Hardin-Pouzet H (2014) Reactive oxygen species are physiological mediators of the noradrenergic signaling pathway in the mouse supraoptic nucleus. *Free Radic Biol Med* 71:231–239
- Rotondo F, Butz H, Syro LV, Yousef GM, Di Ieva A, Restrepo LM, Quintanar-Stephano A, Berczi I, Kovacs K (2016) Arginine vasopressin (AVP): a review of its historical perspectives, current research and multifunctional role in the hypothalamo-hypophysial system. *Pituitary* 19:345–355
- St-Louis R, Parmentier C, Raison D, Grange-Messent V, Hardin-Pouzet H (2012) Reactive oxygen species are required for the hypothalamic osmoregulatory response. *Endocrinology* 153:1317–1329
- Hill JM, Switzer RC 3rd (1984) The regional distribution and cellular localization of iron in the rat brain. *Neuroscience* 11:595–603
- Li C, Odagiri S, Meguro R, Asano Y, Shoumura K (2009) Non-heme-iron deposition in the hypothalamo-neurohypophysial system of the rat brain. *Hiroshima Med J* 60:63–76
- Franklin KBJ, Paxinos G (1997) The mouse brain in stereotaxic coordinates. Academic Press, San Diego
- Meguro R, Asano Y, Odagiri S, Li C, Iwatsuki H, Shoumura K (2007) Nonheme-iron histochemistry for light and electron microscopy: a historical, theoretical and technical review. *Arch Histol Cytol* 70:1–19
- Seo JH, Haam YG, Park SW, Kim DW, Jeon GS, Lee C, Hwang DH, Kim YS, Cho SS (2001) Oligodendroglia in the avian retina: immunocytochemical demonstration in the adult bird. *J Neurosci Res* 65:173–183
- Kim J-H, Jeong EM, Jeong Y-J, Lee WJ, Kang JS, Kim I-G, Hwang Y-i (2012) Transglutaminase 2 modulates antigen-specific antibody response by suppressing Blimp-1 and AID expression of B cells in mice. *Immunol Lett* 147:18–28
- Kim MJ, Kim HK, Chung JH, Lim BO, Yamada K, Lim Y, Kang SA (2005) Increased expression of hypothalamic NADPH-diaphorase neurons in mice with iron supplement. *Biosci Biotechnol Biochem* 69:1978–1981
- Negoescu A, Lorimier P, Labat-Moleur F, Drouet C, Robert C, Guillermet C, Brambilla C, Brambilla E (1996) In situ apoptotic cell labeling by the TUNEL method: improvement and evaluation on cell preparations. *J Histochem Cytochem* 44:959–968
- Tokunaga A, Ono K, Ono T, Ogawa M (1992) Magnocellular neurosecretory neurons with ferritin-like immunoreactivity in the hypothalamic supraoptic and paraventricular nuclei of the rat. *Brain Res* 597:170–175

33. Hansen TM, Nielsen H, Bernth N, Moos T (1999) Expression of ferritin protein and subunit mRNAs in normal and iron deficient rat brain. *Mol Brain Res* 65:186–197
34. Reif DW (1992) Ferritin as a source of iron for oxidative damage. *Free Radic Biol Med* 12:417–427
35. Ray PD, Huang B-W, Tsuji Y (2012) Reactive oxygen species (ROS) homeostasis and redox regulation in cellular signaling. *Cell Signal* 24:981–990
36. Giorgi C, Agnoletto C, Baldini C, Bononi A, Bonora M, Marchi S, Missiroli S, Paternani S, Poletti F, Rimessi A (2010) Redox control of protein kinase C: cell-and disease-specific aspects. *Antioxidants redox signaling* 13:1051–1085
37. Yoshida M (2008) Gene regulation system of vasopressin and corticotropin-releasing hormone. *Gene Regul Syst Bio* 2:GRSB. S424
38. Storici P, De Biase D, Bossa F, Bruno S, Mozzarelli A, Peneff C, Silverman RB, Schirmer T (2004) Structures of gamma-aminobutyric acid (GABA) aminotransferase, a pyridoxal 5'-phosphate, and [2Fe-2S] cluster-containing enzyme, complexed with gamma-ethynyl-GABA and with the antiepilepsy drug vigabatrin. *J Biol Chem* 279:363–373
39. Vega C, Moreno-Carranza B, Zamorano M, Quintanar-Stephano A, Mendez I, Thebault S, Martinez de la Escalera G, Clapp C (2010) Prolactin promotes oxytocin and vasopressin release by activating neuronal nitric oxide synthase in the supraoptic and paraventricular nuclei. *Am J Physiol Regul Integr Comp Physiol* 299:R1701–R1708
40. Yamova L, Atochin D, Glazova M, Chernigovskaya E, Huang P (2007) Role of neuronal nitric oxide in the regulation of vasopressin expression and release in response to inhibition of catecholamine synthesis and dehydration. *Neurosci Lett* 426:160–165
41. Gillard ER, Coburn CG, de Leon A, Snissarenko EP, Bauce LG, Pittman QJ, Hou B, Curras-Collazo MC (2007) Vasopressin autoreceptors and nitric oxide-dependent glutamate release are required for somatodendritic vasopressin release from rat magnocellular neuroendocrine cells responding to osmotic stimuli. *Endocrinology* 148:479–489
42. Bharath S, Hsu M, Kaur D, Rajagopalan S, Andersen JK (2002) Glutathione, iron and parkinson's disease. *Biochem Pharmacol* 64:1037–1048
43. Altamura S, Muckenthaler MU (2009) Iron toxicity in diseases of aging: alzheimer's disease, parkinson's disease and atherosclerosis. *J Alzheimers Dis* 16:879–895
44. Connor JR, Pavlick G, Karli D, Menzies SL, Palmer C (1995) A histochemical study of iron-positive cells in the developing rat brain. *J Comp Neurol* 355:111–123
45. Sturrock RR (1992) Stability of neuron number in the ageing mouse paraventricular nucleus. *Ann Anat* 174:337–340

Publisher's Note Springer Nature remains neutral with regard to jurisdictional claims in published maps and institutional affiliations.